

Accepted Manuscript

An investigation into group 13 (Al, Ga, In) substituted $(\text{Na}_{0.5}\text{Bi}_{0.5})\text{TiO}_3\text{-BaTiO}_3$ (NBT-BT) lead-free piezoelectrics

Ryan McQuade, Thomas Rowe, Alicia Manjón-Sanz, Lilibel de la Puente, Michelle R. Dolgos

PII: S0925-8388(18)31672-4

DOI: [10.1016/j.jallcom.2018.04.329](https://doi.org/10.1016/j.jallcom.2018.04.329)

Reference: JALCOM 45967

To appear in: *Journal of Alloys and Compounds*

Received Date: 9 March 2018

Revised Date: 28 April 2018

Accepted Date: 30 April 2018

Please cite this article as: R. McQuade, T. Rowe, A. Manjón-Sanz, L.d.l. Puente, M.R. Dolgos, An investigation into group 13 (Al, Ga, In) substituted $(\text{Na}_{0.5}\text{Bi}_{0.5})\text{TiO}_3\text{-BaTiO}_3$ (NBT-BT) lead-free piezoelectrics, *Journal of Alloys and Compounds* (2018), doi: 10.1016/j.jallcom.2018.04.329.

This is a PDF file of an unedited manuscript that has been accepted for publication. As a service to our customers we are providing this early version of the manuscript. The manuscript will undergo copyediting, typesetting, and review of the resulting proof before it is published in its final form. Please note that during the production process errors may be discovered which could affect the content, and all legal disclaimers that apply to the journal pertain.



An Investigation into Group 13 (Al, Ga, In) Substituted (Na_{0.5}Bi_{0.5})TiO₃-BaTiO₃ (NBT-BT) Lead-Free Piezoelectrics

Ryan McQuade, Thomas Rowe, Alicia Manjón-Sanz, Lilibel de la Puente, and Michelle R. Dolgos*

Department of Chemistry, Oregon State University, Corvallis, Oregon 97331, United States
Michelle.dolgos@oregonstate.edu

Abstract

Ternary phase diagrams were explored for the systems (Na_{0.5}Bi_{0.5})TiO₃-BaTiO₃-Bi(M)O₃ M=Al, Ga, In to determine periodic trends as a function of substitution. The ferroelectric and piezoelectric properties were measured and compared to (Na_{0.5}Bi_{0.5})TiO₃-BaTiO₃ (NBT-BT). X-ray synchrotron and neutron diffraction data were collected to determine the changes in structure as a function of substitution. Data showed that most systems behave in a similar manner to the parent (Na_{0.5}Bi_{0.5})TiO₃-BaTiO₃. However, two specific compositions display interesting properties: the 2% BiGaO₃ (BG2) substituted sample and the 4% BiAlO₃ (BA4) substituted sample. The BG2 sample undergoes an irreversible electric-field induced phase transition, as seen in NBT-BT, but has a significantly larger high-field strain. The BA4 composition has a different strain mechanism than all the other composition studied. It displays incipient piezoelectricity which results in a giant high-field strain due to a reversible phase transition. This study highlights the difficulty in trying to improve the properties of the highly disordered NBT-BT material.

1. Introduction

Piezoelectric materials are utilized in many commercial devices such as sensors, transducers, and actuators, and the market is continually expanding.[1] Pb(Zr,Ti)O₃ (PZT) is the most common material used in piezoelectric devices due to its high piezoelectric response and the ease with which the properties can be tuned through substitution.[2] Despite the outstanding properties of PZT, it has several disadvantages such as the toxicity of lead, a low operating temperature (below 200 °C), and a susceptibility to fatigue after many cycles.[3–6] One promising material extensively studied for its potential to replace PZT is the solid solution between Na_{0.5}Bi_{0.5}TiO₃ and BaTiO₃, or NBT-xBT. NBT-BT was initially prepared to mimic the rhombohedral-tetragonal morphotropic phase boundary (MPB) where an enhanced piezoelectric effect occurs as demonstrated in PZT (Pb(Zr_{0.52}Ti_{0.48})O₃).[7] While NBT-BT has an established morphotropic phase boundary at approximately 5-7% BaTiO₃, the structural characteristics of the MPB are vastly different from that observed in PZT.[7–9] Under as-synthesized conditions, NBT-BT behaves more like a relaxor ferroelectric, with a broad, frequency-dependent, maximum dielectric permittivity.[7] However, when the sample is poled above its coercive field, it undergoes a structural transition to a ferroelectric structure. At the MPB, this ferroelectric structure is observed up to ~100 °C. At this temperature (T_{F-R}), there is a transition from the ferroelectric to relaxor phase which has a maximum permittivity temperature (T_m) of 288 °C.[10]

The successful manipulation of PZT for use in many applications is in part due to the detailed understanding of its structure-property relationships.[11,12] Unfortunately, the practical use of NBT-BT has not translated to the same success as PZT. The limitations stem from wildly complex short and long-range structures, which results in difficulty when trying to rationally tune its properties.[13]

This work systematically investigates the electromechanical properties of NBT-BT when substituted with group 13 based, bismuth compounds: BiAlO₃ (BA), BiGaO₃ (BG), BiInO₃ (BI). The rationale behind the investigation was to identify any changes in the structure-property relationships as a function of Bi(M)O₃ as M changes down group 13 on the periodic table. None of these three Bi(M)O₃ materials stabilize in the perovskite phase at ambient pressures due to the small size of the Bi³⁺ cation at the A-site. BiAlO₃ and BiInO₃ must be synthesized at high pressures.[14] The perovskite phase of BiGaO₃ is only metastable at high pressures and changes to the pyroxene structure upon decompression.[15] Despite the high pressure requirements for each of these phases, they can stabilize under ambient conditions as a component of a solid solution.[16–19]

Each of these Bi-based perovskites has a noncentrosymmetric space group under certain conditions. BiAlO₃ (Figure 1a) is found in the *R3c* space group and BiInO₃ (Figure 1c) in the *Pna2₁* space group in ambient conditions (after high pressure synthesis).[14] BiGaO₃ (Figure 1b) is found in the space group *Cm* as a coexistent phase between approximately 3 and 6 GPa.[14] However, all three BiMO₃ (M=Al, Ga, In) compounds show promising ferroelectric and piezoelectric properties (M=Al, In), or were predicted to have promising properties (M=Ga).[20,21] In particular, the high Curie temperature (*T_C*) of BiAlO₃ (520 °C) and BiInO₃ (> 550 °C) is attractive as their solid solutions may enhance properties of the ferroelectric regime in NBT-BT. [17,21]

Our study focused on the ternary phase diagram of a Bi(M)O₃ end member (M=Al, Ga, In) with the 0.945Na_{0.5}Bi_{0.5}TiO₃ – 0.055 BaTiO₃ system. Although, BiAlO₃ was substituted into the B-site of NBT-6BT previously, the purpose of our work was to investigate the periodic trends of substituting BA, BG, and BI into NBT-5.5BT.[16,22] We characterized the dielectric, ferroelectric, and piezoelectric properties of (1-x)[0.945Na_{0.5}Bi_{0.5}TiO₃ – 0.055 BaTiO₃] – (x)BiMO₃, with x = 0.02, 0.04 for M=Al³⁺, Ga³⁺ and x = 0.01, 0.02 when M=In³⁺. In addition, preliminary structural studies were performed using synchrotron X-ray and neutron diffraction to aid in understanding the structure-property relationships of these three systems.

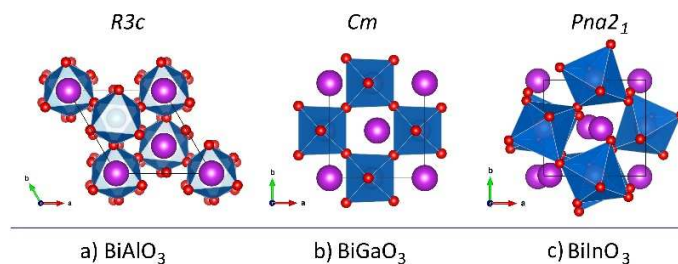


Figure 1: Space groups of group 13, bismuth-based perovskites: a) BiAlO_3 , b) BiGaO_3 , c) BiInO_3 .

2. Experimental

2.1 Synthesis

Group 13 substituted samples of NBT-BT-BM were prepared with the following compositions: $(1-x)[0.945\text{Na}_{0.5}\text{Bi}_{0.5}\text{TiO}_3 - 0.055\text{BaTiO}_3] - (x)\text{BiMO}_3$, with $x = 0.02, 0.04$ for $\text{M}=\text{Al}^{3+}, \text{Ga}^{3+}$ and $x = 0.01, 0.02$ when $\text{M}=\text{In}^{3+}$. For convenience, these compositions are described by the following shorthand notations: NBT-BT-BA2, NBT-BT-BA4, NBT-BT-BG2, NBT-BT-BG4, NBT-BT-BI1, NBT-BT-BI2, and NBT-BT as the parent. Synthesis was performed using standard solid-state methods. The appropriate precursor oxides and carbonates were combined in stoichiometric amounts and ground in an agate mortar and pestle. The precursors used were Bi_2O_3 (Strem Chemicals Inc. 99.999%), Na_2CO_3 (Strem Chemicals Inc. 99.5%), TiO_2 (Cerac Inc. 99.9%), BaCO_3 (Strem Chemicals Inc. 99.9%), Al_2O_3 (Cerac Inc. 99.99%), Ga_2O_3 (Alfa Aesar 99.99%), In_2O_3 (Alfa Aesar 99.9%). All carbonate reagents were dried in a 120°C furnace for at least 48 hours. The mixed powders were ball milled for 6 hours at 350 rpm (10 minutes on, five minutes rest, and 10 minutes in the reverse direction) in a Fritsch Pulverisette 7 with 25 mL of ethanol and eight, 10 mm diameter, yttria-stabilized zirconia balls. The powders were then calcined at 850°C for 2 hours and processed in a vibratory mill for six hours in ethanol with six yttria-stabilized zirconia rods (9.5 mm by 9.5 mm). To further prepare the samples for sintering, they were dried then mixed with a 3 wt % polyvinyl butyral (PVB, Butvar B-98, Sigma Aldrich) binder/ethanol solution. The powder was pressed in a Carver uniaxial press into pellets with a diameter of 13 mm and thickness of ~ 1.5 mm. Pellets were covered in sacrificial powder of the same composition, placed inside capped alumina crucibles and sintered between $1150^\circ\text{C} - 1200^\circ\text{C}$ for two hours (5%/minute ramp rate) depending on the composition. During the temperature ramp up, the temperature was held at 450°C for four hours to remove the PVB binder. All physical properties were measured on pellets with densities greater than 95% of their crystallographic value as determined by a Mettler Toledo Archimedes kit.

2.2 Pellet Processing

Ceramic pellets for physical property measurements were carefully polished to an appropriate thickness of ~1 mm for dielectric measurements and < 0.5 mm for strain (*S-E*) and polarization (*P-E*) measurements. The polishing was completed using a LaboPol-5 (Struers) with #800, #1200, and #4000 SiC foils (Struers). For ferroelectric, room temperature (25 °C - 31 °C) measurements, pellets were painted with silver electrodes (SPI #05002-AB) and dried at 100 °C overnight. For temperature dependent dielectric measurements, electrodes of high-temperature silver paint (Heraeus C1000 HT) were applied to the parallel faces of each pellet before the pellet was heated to 750 °C for 30 minutes to cure the silver electrodes.

2.3 Physical Properties Measurements

Dielectric permittivity was measured using an HP 4192A LF Impedance Analyzer, a NorECsAS ProbostatTM, and a Carbolite tube furnace. The measurements were performed during cooling on both poled and unpoled samples as a function of temperature from 1 kHz to 1 MHz, from RT (room temperature, 25-31 °C) to 550 °C at a 2 °C /min ramp rate. Strain vs. electric field (*S-E*) and polarization vs. electric field (*P-E*) measurements were performed on a Radiant Precision Premier II, at a frequency of 0.1 Hz and 1 Hz respectively, with the sample pellet submerged in an insulating silicone oil. Poling was performed on the Radiant Precision Premier II at 50 kV/cm for 30 minutes at room temperature (25 °C). After 24 hours, the direct piezoelectric effect was measured on a Berlincourt-type d_{33} meter (APC International, Ltd. YE2730A). Also after the 24-hour resting period, the converse piezoelectric properties were measured using the Radiant Precision Premier II connected to an optical displacement MTI-2100 Photonic Sensor.

2.4 Diffraction Experiments

Phase purity of each sample was verified using X-ray diffraction (XRD) on a Rigaku Miniflex 600 (Cu $K\alpha$, $\lambda = 1.541862$ Å, 2θ range from 10 to 65 °). XRD comparisons of poled and unpoled powder samples were also performed on the Rigaku Miniflex 600 (Cu $K\alpha$, $\lambda = 1.541862$ Å, 2θ range from 20° to 60°, 0.625° incident slit, 5° soller slit). Crushed powders were annealed at 450 °C for three hours. Synchrotron X-ray diffraction (SXR) data were collected at the Advanced Photon Source at Argonne National Laboratory on the 11-BM beamline.[23] Samples were ground lightly with a mortar and pestle, annealed to relieve the stress from grinding, then loaded into quartz capillaries. Each sample was diluted with quartz wool to avoid absorption phenomena. Data were collected at room temperature for one hour in the 2θ range of 0.5 to 50 at a wavelength of 0.459980 Å.

Neutron powder diffraction (NPD) data were collected at Oak Ridge National Laboratory on the POWGEN diffractometer. Approximately 3 grams of each sample was loaded into vanadium containers and one-hour scans were performed at room temperature using a wavelength of 1.066 Å (d -spacing range of 0.276-4.606 Å).

Pawley fits were performed using Topas Academic software.[24] Neutron, two-phase refinements were performed with six Chebyshev background terms, a t.o.f. sample peak shape function, and FWHM terms to adjust peak widths. For the APS, XRD data, six background terms were used as well as the Stephen's broadening model for monoclinic and tetragonal phases. Four Pseudo-Voigt terms were used to fit background with the diffuse scattering and contributions from the quartz wool.

3. Results and Discussion

3.1 Dielectric Properties

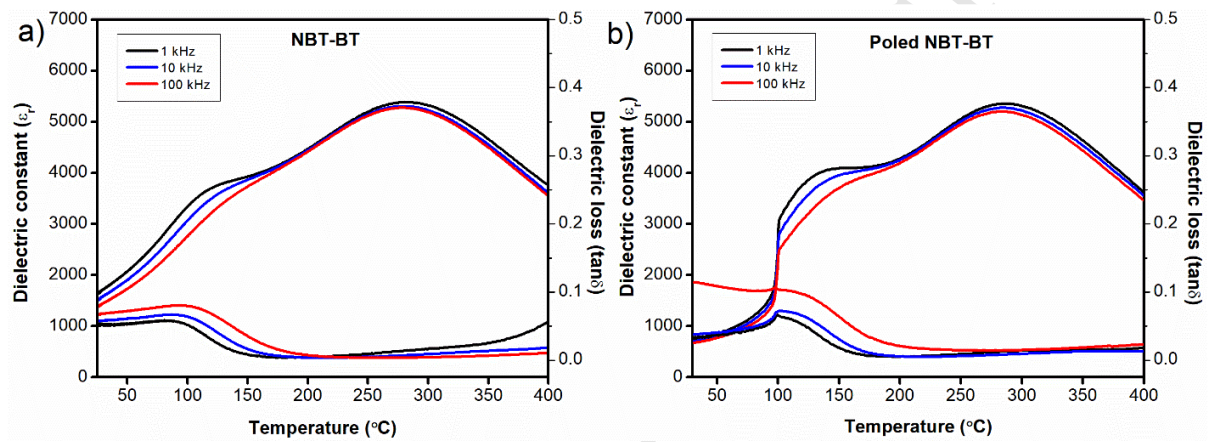


Figure 2: Temperature dependence of the dielectric permittivity and $\tan \delta$ of both a) unpoled and b) poled NBT-5.5BT.

Table 1: Summary of dielectric properties of unpoled samples.

Composition	ϵ_r at T_m	T_m (°C)	ϵ_r^\dagger	$\tan \delta^\dagger$	T_{F-R} (°C)
NBT-BT	5333	288	1640	0.0523	99
NBT-BT-BA2	5456	258	1805	0.0547	75
NBT-BT-BA4	4224	243	1617	0.0533	46
NBT-BT-BG2	6626	259	1827	0.0559	94
NBT-BT-BG4	4616	252	1525	0.0515	80
NBT-BT-BI1	5537	284	1512	0.0475	70
NBT-BT-BI2	4520	289	1336	0.0495	71

† Dielectric data obtained at room temperature with a frequency of 1 kHz.

All data reported at a frequency of 1 kHz.

3.1.1 NBT-BT

The dielectric permittivity and loss of the parent sample, NBT-BT, are shown in Figure 2a. Two dielectric features, typical of this composition were observed: a shoulder peak at $\sim 115^\circ\text{C}$ which has caused much confusion in the literature, and a large, broad peak at 288°C , which is referred to as the maximum permittivity temperature, T_m . The large, frequency- dependent,

diffuse peak is typical of relaxors and arises from the size and distribution of polar nano-regions (PNRs).[25] The shoulder peak is a debated phenomenon, but we agree with the study by Jo et al. attributing the anomaly to the thermal evolution of an increasing number of rhombohedral ($R3c$) to tetragonal ($P4bm$) PNRs.[26–28] We observed both of these dielectric features in varying degrees in both the parent and substituted samples.

As mentioned previously, NBT-BT undergoes a ferroelectric-relaxor transition under the application of an electric field. Therefore, the ferroelectric-relaxor transition temperature, denoted as T_{F-R} , was investigated by poling samples above their coercive field before measuring the dielectric permittivity as a function of temperature. At T_{F-R} , the thermal energy disrupts the correlated FE domains.[29,30] Above T_{F-R} , broad, frequency dependent peaks, typical for relaxor ferroelectrics, are observed.[31] T_{F-R} was determined from the complementary peak maximum in the loss at 1 kHz. Previously, this peak in $\tan \delta$ was used to label the depolarization critical temperature, T_d , but recent studies define this temperature as the ferroelectric-relaxor temperature (T_{F-R}).[26] T_{F-R} not only describes where this transition occurs, but it also provides insight into how strongly the FE domains are coupled together. It is generally 5-20 °C higher than the depolarization temperature, T_d , as measured by TSDC (thermally stimulated depolarization current).[26,28] For the parent sample, NBT-BT, the T_{F-R} was measured at 99 °C, a temperature consistent with reported values.[32] All the dielectric data for NBT-BT as summarized in Table 1 agree with previous work.[7,33]

3.1.2 Unpoled NBT-BT-Bi(M)O₃

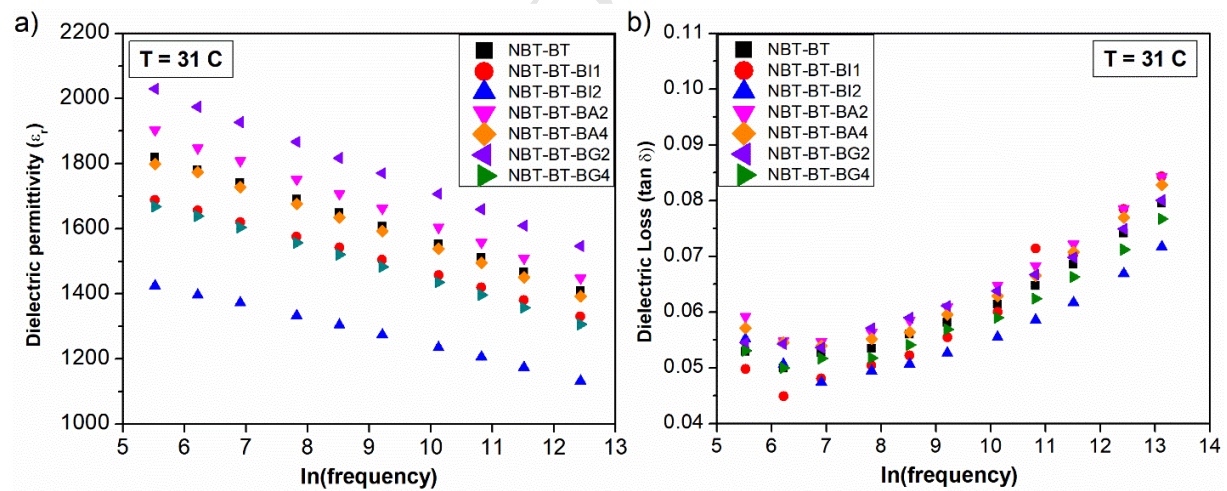


Figure 3: Frequency dispersion data of (a) dielectric permittivity and (b) dielectric loss from unpoled samples at 31 °C.

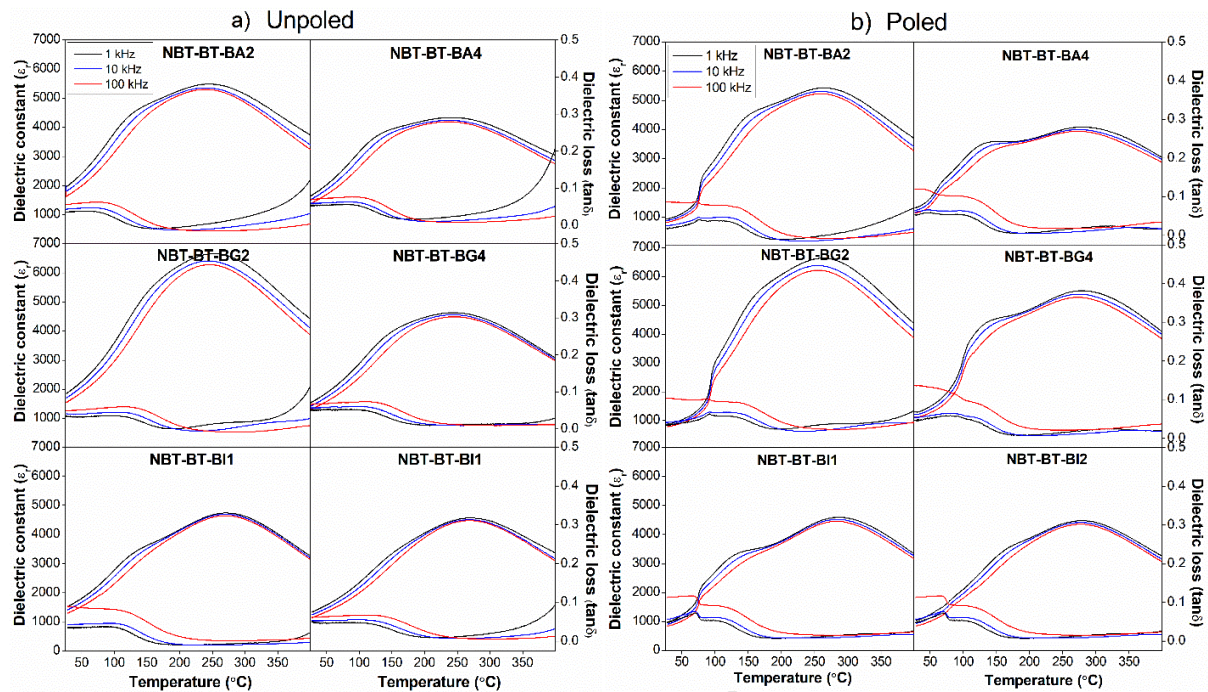


Figure 4: Temperature dependence of the dielectric permittivity and $\tan \delta$ of both a) unpoled and b) poled samples.

The frequency dependence of the room temperature dielectric permittivity (ϵ_r) is shown in Figure 3a. The frequency dependence is evident across all compositions in the dielectric permittivity, indicating their relaxor nature. NBT-BT-BG2 and NBT-BT-BA2 display a higher permittivity at room temperature compared to the parent compound, with permittivity values of 1827 and 1805 respectively (at 1 kHz). In addition, their frequency dispersion is larger than NBT-BT (Table A1). The remaining substituted compounds have a lower RT permittivity than NBT-BT and their frequency dispersion is slightly smaller than that of the parent compound.

The loss ($\tan \delta$) at RT also shows frequency dispersion across all samples with lower frequencies having lower loss than higher frequencies (Figure 3b). NBT-BT-BA2, NBT-BT-BA4, and NBT-BT-BG2 have dielectric losses of 0.0547, 0.0533, and 0.0559 respectively, at 1 kHz. These loss values are higher than NBT-BT at 0.0523, but fairly typical of lead-free piezoelectrics.[34,35] NBT-BT-BI1 has the lowest loss at lower frequencies (0.05 at 10 kHz) and the highest at higher frequencies (0.0843 at 500 kHz) while NBT-BT-BI2 shows the lowest loss across all other frequencies (0.03 at 10 kHz).

The temperature dependent dielectric permittivity and loss of each unpoled composition is shown in Figure 4a with the data summarized in Table 1. The substituted compounds retain the relaxor features found in NBT-BT including the prominent shoulder feature observed in varying degrees for all new compositions. However, continued substitution results in a lowering of the permittivity and this shoulder becomes more convoluted into the diffuse dielectric peak.

In general, when $M = \text{Al}$ or Ga , the dielectric permittivity (ϵ_r), ϵ_r at T_m , and $\tan \delta$, initially increase upon addition of Bi(M)O_3 , then decrease with further substitution. These trends

indicate that there is some critical composition between 2% and 4% BA and BG that could possess the best ferroelectric and piezoelectric properties in those systems. Specifically, the NBT-BT-BA system demonstrates the best dielectric performance at ~2% BA, which corresponds to the reported critical MPB composition.[16,22] The trends in the $M = \text{In}$ compositions are more complicated. For the In family, ϵ_r at T_m , T_C , and $\tan \delta$ increase with initial substitution, then decrease upon further addition, as in the Al and Ga systems. However, the trend with the In compounds varies in that ϵ_r decreases and T_m remains constant as more BiInO_3 is added.

3.1.3 Poled

All compositions were poled as described above to determine if an electric-field induced phase transition to a ferroelectric structure occurs as seen in the parent compound. It was observed that all samples, to varying degrees, undergo this transition where the electric field creates a ferroelectric state. Therefore, the dielectric permittivity of the poled samples deviates from the unpoled samples in the form of a frequency-independent vertical alignment of the permittivity data until the approximate temperature of the transition from a poled ferroelectric to a relaxor state. These poled materials remain ferroelectric up to the critical temperature, T_{F-R} , then display characteristics of ergodic relaxors, such as the inability to be poled and low remnant polarization. In each system, T_{F-R} significantly decreases with increasing addition of the BiMO_3 component.

The dielectric data indicates that all the compositions display non-ergodic relaxor behavior below the ferroelectric-relaxor temperature (T_{F-R}). The polar nano-regions in nonergodic phase regions are ‘frozen’ and can be poled so they display a strain response similar to other poled piezoelectric ceramics. The mechanism of the strain response is derived from an irreversible phase transition under an electric field from the nonpolar phase to a long-range ferroelectric structure. Above T_{F-R} the materials transition to an ergodic state where the PNRs are mobile and the material loses the ability to retain long-range, concerted, polarized domains.[36–38] In a non-polar, or weakly polar, ergodic phase, the material may become ferroelectric as they undergo a phase transition to a long-range polar structure induced by the applied electric field. However, unlike in the non-ergodic state, this transition is reversible, as the difference between the free energy of the competing phases is small.[16,36] Therefore, once the field is removed, the material returns to the unpoled, non-polar phase.

Substitution has the most profound impact on the dielectric properties in the BA series. The addition of BiAlO_3 resulted in increased disorder and the T_{F-R} drastically lowered to near room temperature. The change in permittivity behavior is accompanied by a decrease in the sharpness of the T_{F-R} loss peak ($\tan \delta$), making it difficult to determine the exact point the transition begins (reported at the peak of the 1 kHz $\tan \delta$). As the T_{F-R} approaches RT with increasing substitution, the material will become more difficult to pole. This phenomenon is shown in the NBT-BT-BA4 sample where only the diffuse remnants of the transition remain in the loss peak data. Continued substitution would likely continue to decrease this transition temperature below room

temperature. A T_{F-R} , at or near RT like that observed in the BA4 composition, could potentially display incipient piezoelectric properties that demonstrate giant strain which could be utilized in actuator devices.[39]

The trend shown in the NBT-BT-BG system is similar to that found in NBT-BT-BA. However, it is difficult to determine the transition with NBT-BT-BG4 as the peak in loss indicating T_{F-R} appears more diffuse than in other samples. It does appear that the decrease in T_{F-R} as a function of substitution is not nearly as dramatic in NBT-BT-BG compared to the BA system. A 4% BiGaO₃ substitution decreases the T_{F-R} by ~20 °C compared to a ~50 °C degree decrease with the BiAlO₃ end-member. This difference demonstrates that aluminum substitution more readily interrupts the correlation length of the PNRs compared to gallium. This could possibly result from the lower polarizability of aluminum.

It is more difficult to clearly determine the dielectric properties of the poled NBT-BT-BI system. NBT-BT-BI2 displays a T_{F-R} peak in the loss data, but evidence of the transition in the real permittivity is lacking with only a slight anomaly left over from the poling state. The BiInO₃ system shifts T_{F-R} down approximately 30 °C and, just like the BiAlO₃ and BiGaO₃ systems, the trend remains consistent with increased compositional substitution. Unfortunately, it is difficult to discuss any trends in these interesting compositions as BiInO₃ has such a low solubility in the parent system.

3.2 Piezoelectric Properties

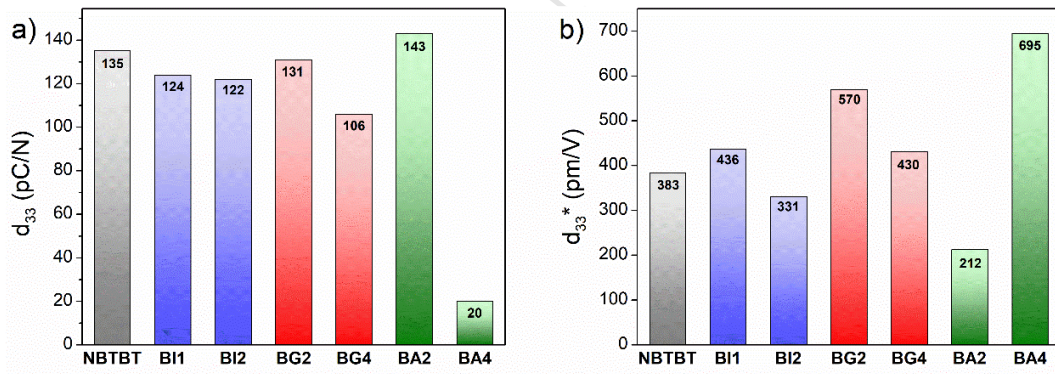


Figure 5: Piezoelectric coefficients, a) d_{33} , b) d_{33}^* ($d_{33}^* = S_{\max}/E_{\max}$), for all compositions. The gray bar represents parent system, blue bars represents the BI system, red represents the BG system, and green represents the BA system.

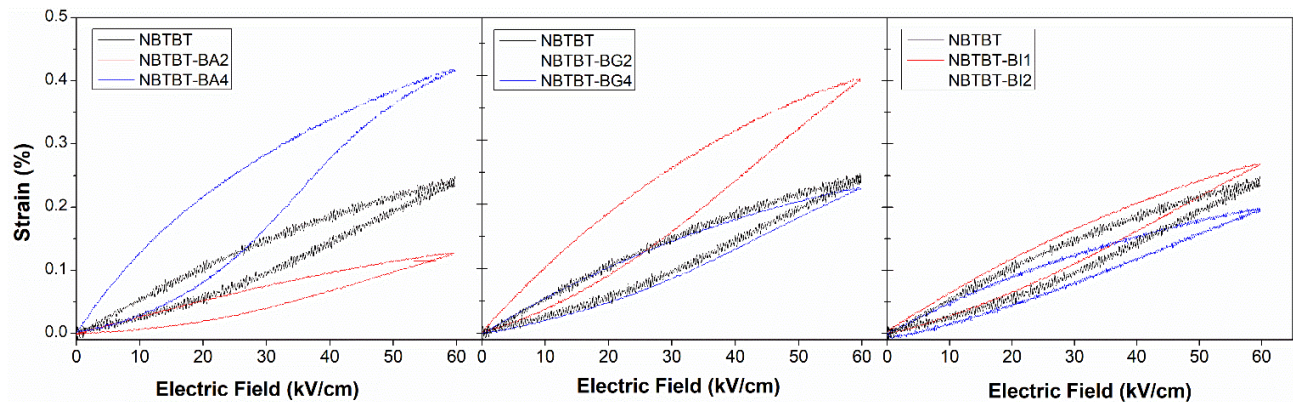


Figure 6: High-field, unipolar strain measurements (S - E) for each composition compared to the parent, NBT-BT.

The direct piezoelectric effect was measured on poled samples of all compositions, with the results shown in Figure 5a. The d_{33} of the parent compound NBT-BT was determined to be 135 pC/N, which falls within the reported values in the literature.[7,22] Most of the substitutions of NBT-BT such as the BI compositions, NBT-BT-BG2 and NBT-BT-BA2 have little effect on d_{33} . Two of the samples show a significant decrease in d_{33} . The d_{33} of NBT-BT-BG4 decreases 20% to 106 pC/N and the d_{33} of NBT-BT-BA4 decreased 85% to 20 pC/N.

Unipolar (Figure 6), strain-electric field measurements (S - E) were performed on all compositions to determine their maximum strain and their high field piezoelectric response, d_{33}^* (Figure 5b), which indicate their potential for use in actuator applications. A sample of other reported d_{33} values for the NBT-BT system is shown in Table A2.

The maximum strain for NBT-BT was measured at 60 kV/cm for the unipolar loops. In the BG and BI families, initial substitution increases the high-field strain, while further substitution causes the strain to decrease to values similar to or below that of the parent composition NBT-BT. This trend is much more pronounced in the BG materials, while the addition of BI does not significantly affect the strain properties. In the BA series, the strain decreases dramatically ($d_{33}^*=212$ pm/V) with the first substitution then increases significantly above the value of the parent with the second substitution ($d_{33}^*=695$ pm/V). The d_{33}^* of the NBT-BT parent is 383 pm/V. The effect of substitution on d_{33}^* mirrors the trends in the strain results where NBT-BT-BA4 shows the largest increase in d_{33}^* to 695 pm/V and NBT-BT-BG2 also shows a significant improvement to 570 pm/V. The piezoelectric property results are listed in Table 2.

The BI data show that BI substitution has little impact on the electromechanical properties of NBT-BT. A small amount of BG substitution, however, improves the maximum strain and d_{33}^* significantly. Although, this substitution has little impact on d_{33} . A more detailed investigation of this system is underway to determine if the strain is related to the incipient piezoelectric mechanism. The BA system has the most interesting changes in the piezoelectric properties due to substitution. The piezoelectric data for the BA4 compound shows that this material can be classified as an incipient piezoelectric. An incipient piezoelectric displays an electric-field dependent, giant strain where the contributing mechanism is through a phase transition from a paraelectric to ferroelectric structure. Unlike the phase transition observed in the parent NBT-

BT, this mechanism is reversible and the structure reverts to the paraelectric phase upon removal of the electric field.[38]

In 2007, Zhang et al. reported on one of the earliest known ergodic relaxors showing incipient piezoelectricity. They found a giant strain in NBT-BT-KNN ($\text{K}_{0.5}\text{Na}_{0.5}\text{NbO}_3$) of 0.45% (567 pm/V at 80 kV/cm) accompanied by a reduced direct d_{33} measurement of 30 pC/N.[40] This giant strain is only activated above a certain electric field with a very large hysteresis and also only occurs when the direct piezoelectric behavior is severely diminished.[41,42] This same effect is seen in this BA4 sample where the high field d_{33}^* is 695 pm/V and the macroscopic piezoelectric response d_{33} is only 20 pC/N. The literature shows this giant strain can often be encouraged with small substitutions in NBT-BT and BNT-BKT ($\text{Bi}_{0.5}\text{Na}_{0.5}\text{TiO}_3$ - $\text{Bi}_{0.5}\text{K}_{0.5}\text{TiO}_3$) based systems.[35,38,43] Giant strain with d_{33}^* values up to 1400 pm/V have been shown for some bismuth based systems, such as $((\text{Bi}_{0.5}(\text{Na}_{0.84}\text{K}_{0.16})_{0.5})_{0.96}\text{Sr}_{0.04})(\text{Ti}_{0.975}\text{Nb}_{0.025})\text{O}_3$. [44] For pure NBT-BT based systems, reported values range from ~500-700 pm/V (values in Table A2). This NBT-BT-BA system displays a strain of 695 pm/V which is near the high-end of these reported values.

In the parent compound and in all other samples, the bipolar strain-field data display a butterfly loop as shown in Figure 7. The loop has both a positive and negative component, which results from ferroelectric domain switching.[38] However, the strain-field of an incipient piezoelectric, is described as a “sprout-like” shape with no negative switching component due to the reversibility of the phase transformation back to a paraelectric phase after removal of the field. This sprout-like loop is observed in the BA4 sample only (Figure 4d), while the NBT-BT and all other compositions display a typical piezoelectric strain-field loop (Figure A3).

This behavior in BA4 can be explained by the low $T_{\text{F-R}}$ transition temperature at ~45 °C, which is significantly lower than that of all the other compositions. This composition appears to show properties of an ergodic relaxor, despite a $T_{\text{F-R}}$ above room temperature. One possible explanation for this is that the $T_{\text{F-R}}$ reported might not be accurate. $T_{\text{F-R}}$ is determined by the peak in dielectric loss ($\tan \delta$), which for this BA4 composition appears diffuse, making it difficult to pinpoint the exact maximum of the peak. An alternative explanation is the sample has a distribution of transitional ferroelectric to relaxor temperatures deriving from the coexistence of ergodic and nonergodic phases.[45] Combined ergodic and nonergodic regions may also explain the weak, diffuse peak in the dielectric loss.

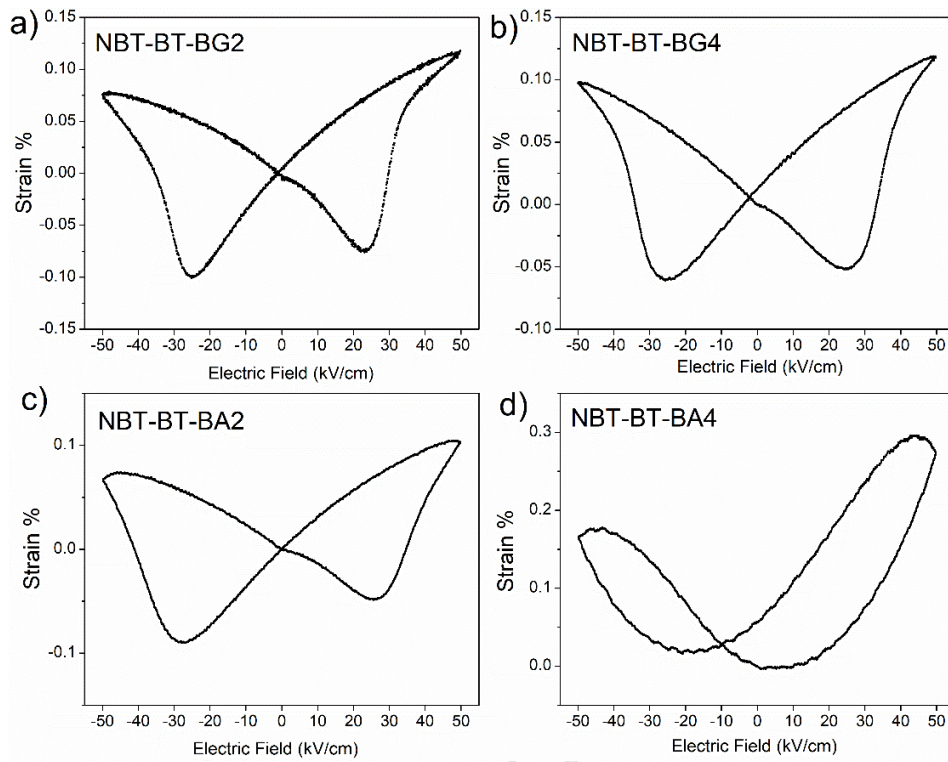


Figure 7: Bipolar, S-E (BSE) loops of a) NBT-BT-BG2, b) NBT-BT-BG4, c) NBT-BT-BA2, and d) NBT-BT-BA4 at 50 kV/cm.

3.3 Ferroelectric Properties

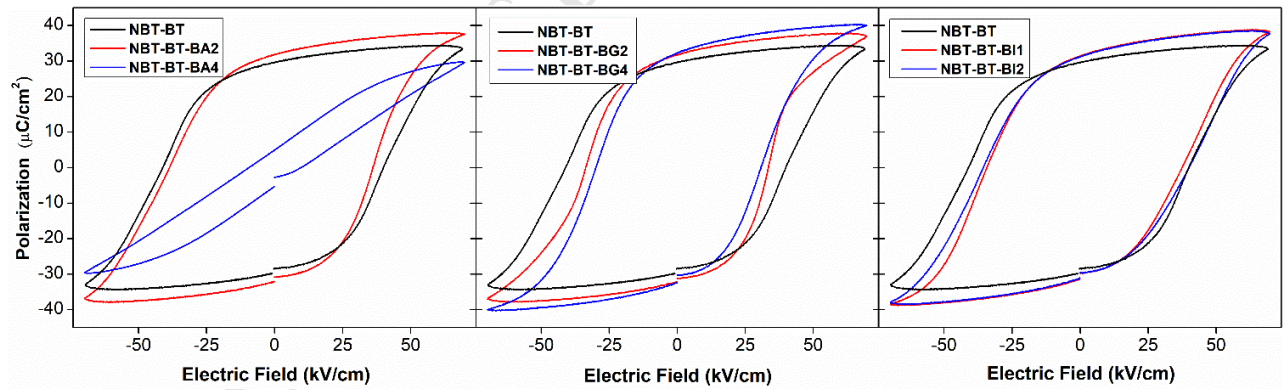


Figure 8: Polarization vs. electric field, ferroelectric, hysteresis loops for the parent composition plotted with each of the two substituted samples in each system for comparison (freq = 1kHz, 70 kV/cm).

Table 2: Summary of ferroelectric and piezoelectric properties.

Composition	P_m ($\mu\text{C}/\text{cm}^2$) †	P_r ($\mu\text{C}/\text{cm}^2$) †	E_c (kV/cm) †	d_{33}^* (pm/V) ††	d_{33} (pC/N) ††
NBT-BT	33.4	29.7	39.9	383	135
NBT-BT-BA2	36.1	31.2	38.1	212	143
NBT-BT-BA4	29.6	4.95	9.6	695	20
NBT-BT-BG2	37.1	31.7	33.2	570	131
NBT-BT-BG4	40.1	32.2	29.5	430	106
NBT-BT-BI1	38.4	31.3	35.2	436	124
NBT-BT-BI2	37.8	31.2	37.1	331	122

† Ferroelectric data obtained at room temperature with a frequency of 1 kHz.

†† Strain measurements obtained at room temperature with a frequency of 0.1 kHz.

$d_{33}^* = S_{\text{max}}/E_{\text{max}}$; where S_{max} is observed at maximum field.

Ferroelectric, polarization-electric field measurements (P - E) were performed at room temperature and are shown in Figure 8 for all samples at fields of 70 kV/cm. The ferroelectric property results are summarized in Table 2.

Based on the saturated P - E hysteresis data, the NBT-BT-BG and NBT-BT-BI systems perform as typical ferroelectric materials with only incremental increases in the ferroelectric properties of remnant polarization (P_r) and maximum polarization (P_m). In the NBT-BT-BG system, both substitutions perform similarly in P - E measurements. NBT-BT-BG2 shows an ~11 % increase in P_m , a ~7 % increase in P_r , and a decrease of ~17 % in the coercive field (E_c), compared to the NBT-BT parent. Further substitution of BG beyond 2 % marginally increases the polarization and lowers the coercive field a further 12 %. The inclusion of 1 % and 2 % BiInO_3 into the parent NBT-BT system only slightly improves the polarization response. NBT-BT-BI1 shows an increase in remnant polarization of ~5 % and an increase in maximum polarization of ~13 %. The coercive field decreases by ~11 % compared to the parent compound's 39.9 kV/cm. NBT-BT-BI2 has a ~5 % higher remnant polarization, while the maximum polarization increases by ~13 %, and the coercive field of decreases ~7 %, compared to the parent compound.

The NBT-BT-BA system behaves differently than the BG and BI systems. The NBT-BT-BA2 sample performs similarly to the parent, but NBT-BT-BA4 clearly deviates from all other compositions. The shape of the hysteresis loop of NBT-BT-BA4 more closely resembles a relaxor in the ergodic phase region. The remnant polarization drops to 4.95 $\mu\text{C}/\text{cm}^2$ as the long-range ferroelectric ordering is destroyed upon the removal of the electric field. This evidence compliments the piezoelectric and dielectric properties observed above and supports the giant strain in this composition coming from an incipient piezoelectric effect.

4. Structure

4.1 X-ray and Neutron Diffraction Analysis

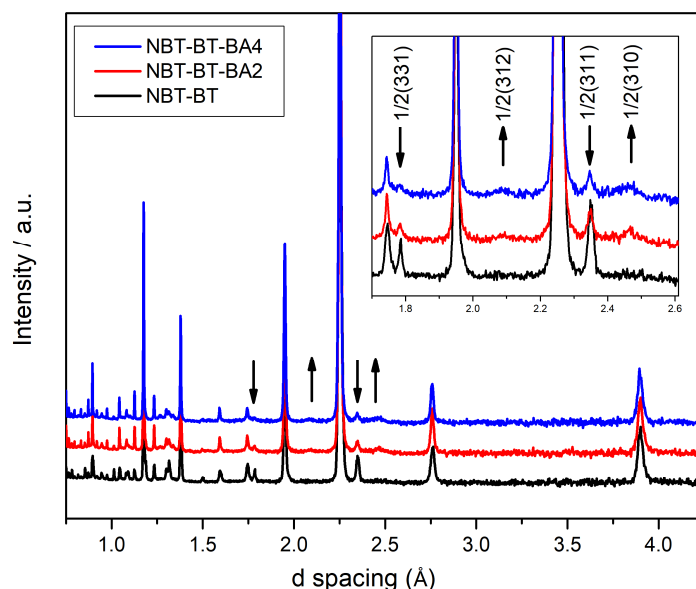


Figure 9: Overlaid NBT-BT, NBT-BT-BA2, NBT-BT-BA4 neutron diffraction patterns showing increasing and decreasing superlattice reflections.

All synthesized ceramics exhibit a pseudo-cubic perovskite structure with no impurity phases present. While both synchrotron x-ray (Figure A4) and neutron diffraction (Figure 9) data were collected, the neutron data provides more useful information due to the subtle structural effects of the oxygen atoms and the pseudocubic nature of the x-ray diffraction. Therefore, the bulk of this discussion will focus on the neutron data.

All three substitutions display the same trends in both their diffraction patterns. While the nature of the structure of NBT-BT is debated in the literature (Table A5), we found both NBT-BT and the substituted compounds crystallize into two polar phases: $P4bm$ and Cc . The base-centered, monoclinic space group, Cc , has a Glazer tilt system of $a^-a^-c^+$, and a polarization plane between the tetragonal $[001]$ and rhombohedral $[111]$, with possible directions of $[uuv]$.^[46,47] This space group is also the structure of the end-member $\text{Na}_{0.5}\text{Bi}_{0.5}\text{TiO}_3$.^[48,49] The primitive, tetragonal $P4bm$ has a tilt system of $a^0a^0c^+$ and a polarization direction of $[001]$.^[46,50] It has been suggested the complexity of the diffraction data could stem from more complex tilting arrangements than can be described by Glazer notation.^[33] This two-phase, monoclinic-tetragonal model is similar to previously reported models and no other dual-phase refinement was as successful fitting the data.^[48] Other common combinations that have been reported in the literature were considered during the analysis: Cc , $Cc + R3c$, $Cc + Pm\bar{3}m$, $R3c + P4bm$, $R3c + P4mm$ (Table A5), but they either missed some of the observed peaks or they did not fit the intensity profiles of the data and returned higher residual values than the selected Cc and $P4bm$ space groups.^[33,34,48,51,52] However, we do want to point out that conflicts between our

assigned space groups and some reports in the literature are to be expected. These materials display a complex microstructure and are sensitive to synthesis and handling conditions.[31,33,53]

Substitution does not change the number of reflections from the parent compound in the diffraction patterns. However, the patterns of the substituted compositions clearly exhibit increases to the intensity of a series of peaks related to *P4bm* superlattice reflections. These superlattice reflections originate from the doubling of the unit cell due to octahedral tilting. Typically, the $\frac{1}{2}$ (00e) (Miller indices of odd, odd, even), superlattice reflections are assigned to the *P4bm* space group and the $\frac{1}{2}$ (00o) double cell reflections are assigned to the rhombohedral *R3c*. [33,54] Our refinements assign the $\frac{1}{2}$ (00o) reflection to the monoclinic *Cc*, which also displays these superlattice reflections.[46] The short, broad nature of the *P4bm* supercell reflections could be explained by the lamellar nature of the tetragonal phase observed in these systems.[55,56] While the relative fraction of *P4bm* increases with substitution, the degree of tetragonality remains essentially unchanged with a *c/a* ratio of 0.998 based on the Pawley fits from the neutron diffraction data (Table A6). The neutron diffraction pattern also reveals a decrease in the monoclinic phase, which is evident in the decrease in the series of peaks in Figure 9. While the tetragonality doesn't change significantly upon substitution, the a_m/b_m ratio, increases from 1.735 in NBT-BT to 1.751-1.772 in the indium and aluminum compositions (Table A6). The value of this ratio is $\sqrt{3}$ (1.732) in a rhombohedral structure and the deviation from this ratio describes the monoclinic distortion of the unit cell.[57] What these Pawley fits show is that the distortions in both monoclinic and tetragonal structures are relatively small, resulting in the pseudocubic diffraction patterns typical of relaxor ferroelectrics.

While Rietveld refinements were performed on the neutron data, full structural models were inconclusive due to unstable models that could not be identified as absolute minima. Many factors lead to the challenging assessment of the average structure: a tetragonal phase with small, broad peaks; negative thermal displacement parameters for a few oxygen sites, and local distortions that lead to a large amount of diffuse scattering. Additional cations introduced into the NBT-BT system in this study further increase disorder, which manifests itself with an average pseudocubic structure that is typical of relaxors, but notoriously difficult to model.[13,25,31,58] Our refinements were similar to the results by Ge et al., where an example refinement can be found in the SI (Table A7 and Figure A8).[48] However, in the case of both NBT-BT and its substituted constituents, the extent of disorder prevents a clear description of the structure with diffraction data alone.

4.2 Poled/Unpoled

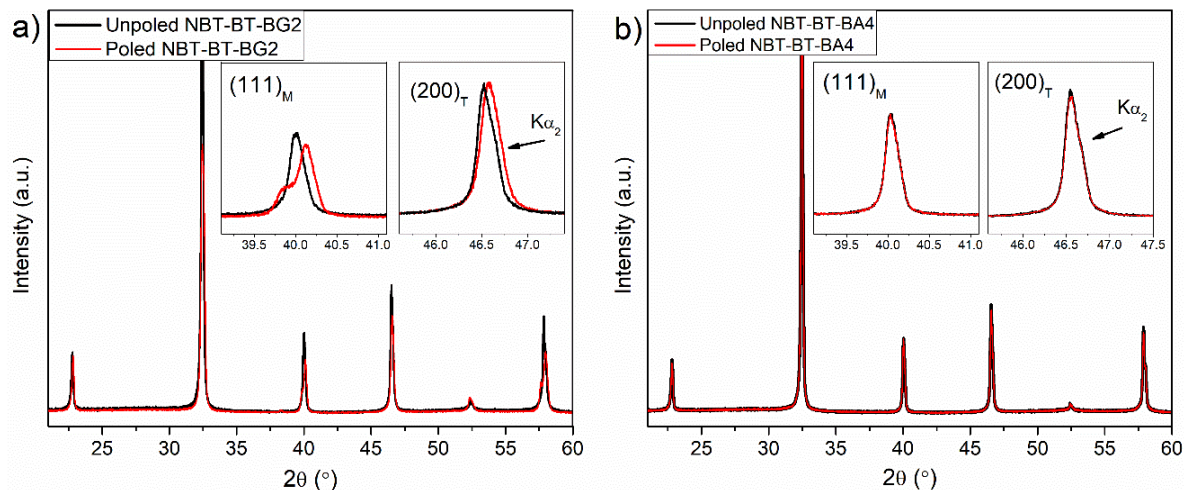


Figure 10: Laboratory x-ray diffraction data for crushed pellets of a) NBT-BT-BG2, unpoled and poled and b) NBT-BT-BA4, unpoled and poled. Inset expands the $(111)_M$ and $(200)_T$ reflections which can demonstrate monoclinic and tetragonal splitting, respectively.

X-ray diffraction data was collected on poled samples of the two compositions with the highest strain response, NBT-BT-BG2 and NBT-BT-BA4, to further understand the origin of their strain mechanisms. This diffraction data will provide more information about the nature of any electric-field induced structural changes. Recall that the BG2 composition shows a large strain while the d_{33} remains similar to that in the parent compound, while the BA4 composition demonstrates properties inherent to an incipient piezoelectric where the strain increases dramatically while the d_{33} decreases sharply. We show that NBT-BT-BA4 is an incipient piezoelectric that shows a reversible transition with a high strain only at high electric fields, while the other compositions behave like NBT-BT where a phase transition upon poling results in increased long-range ferroelectric ordering and high piezoelectric strain.

The poled NBT-BT-BG2 diffraction data in Figure 10 shows a clear structure change compared to the unpoled sample. Splitting of the $(111)_M$ is indicative of the formation of a more highly distorted monoclinic phase from the more symmetric, pseudocubic phase. The peak-splitting observed for the monoclinic $(111)_M$ peak shows an increase in the long-range ferroelectric ordering that emerges from the applied electric field.[16] The lack of significant changes in the $(200)_T$ peak implies little change in the tetragonal phase upon poling. We hesitate to comment further about what the specific changes occur to both phases upon poling as this diffraction data was collected on a laboratory based XRD. To understand the structural mechanism of poling, both neutron diffraction data, which is sensitive to oxygen positions, and high energy X-ray diffraction data, which allow for better peak resolution, should be collected and analyzed. The poled structure of NBT-BT was not fully understood to show changes in both phases until neutron diffraction was performed.[59–61] Therefore, for now we can only say that there is a clear structural transition after poling in the BG2 composition. This structural change

as a function of electric field is supported by strong FE polarization-electric field measurements as well as piezoelectric strain curves with large negative strain indicating ferroelectric switching.

In contrast, there is no discernable difference in the XRD patterns of poled and unpoled NBT-BT-BA4. In Figure 10b, there is clearly no splitting or peak shifts in the featured $(111)_M$ and $(200)_T$ peaks. As discussed previously, the strain originates from the ferroelectric phase that is induced at high electric fields, but reverses back to the pseudocubic structure when the electric field is removed. Near room temperature, the material is dominated by its paraelectric-ergodic nature which is demonstrated by the low T_{R-F} of this composition. As the boundary between the nonergodic and ergodic phases is approached, the long-range ferroelectric domains cannot be achieved as a permanent phase transition as a function of electric field. The high field ferroelectric domains relax back to their PNR states when the field is removed and therefore do not display a structural change after poling. This structural description is supported by the lack of direct strain (d_{33} , Figure 5a), the lack of negative strain in the bipolar strain curves (Figure 7d), and the polarization-electric-field measurements (Figure 8).

5. Conclusion

When considering the dielectric, ferroelectric, and piezoelectric properties, no obvious trends can be described down the group in the periodic table as the third component of the phase diagram changed from BiAlO_3 to BiInO_3 . The BI and BG systems behaved similarly to the parent compound NBT-BT where the mechanism for a large strain and d_{33} come from an electric-field induced phase transition where the long-range ferroelectric ordering is increased. In the Al system, a large strain and high field d_{33} were observed, but showed a significant decrease in the macroscopic ferroelectric properties and the low field d_{33} . The strain mechanism in the Al system is very different from that observed in all the other compositions and is derived from incipient piezoelectricity. In this case, a reversible phase transition which increases ferroelectric ordering at high fields results in a large strain and high-field d_{33} . When the field is removed, the long-range ordering relaxes back into a pseudocubic structure resulting in diminished macroscopic properties. Unfortunately, the applied field necessary to achieve the high strain ($\sim 7\text{kV/mm}$) is likely too high for long term, reliable usage. However, this example shows how non-polar groups with an incipient piezoelectric strain mechanism could be useful in applications if the applied electric field to achieve the giant strains is reasonable.

Conflict of Interest

The authors have no conflicts of interest to declare.

Acknowledgements

Michelle Dolgos and Alicia Manjón-Sanz would like to thank the NSF for support (DSF-1606909). The authors also thank Oregon State University for additional funding and use of instruments. Use of the Advanced Photon Source at Argonne National Laboratory was supported by the U. S. Department of Energy, Office of Science, Office of Basic Energy Sciences, under Contract No. DE-AC02-06CH11357. A portion of this research used resources at the Spallation Neutron Source, a DOE Office of Science User Facility operated by the Oak

Ridge National Laboratory. We would like to thank Saul Lapidus at 11-BM (APS) and Pam Whitfield, Ashfia Huq, and Melanie Kirkham of POWGEN (SNS) for their assistance and support in collecting high quality diffraction data. The authors would like to thank David Cann of the Materials Science division at Oregon State University, as well as Nitish Kumar, Noon Prasertpalichat, and Nopsiri Chaiyo for access to instrumentation and informative discussions about the complex world of relaxor ferroelectrics.

References

- [1] T. Abraham, Expanding Markets for Piezoelectrics Markets., 2014.
<http://www.ceramicindustry.com/articles/93845-expanding-markets-for-piezoelectrics>.
- [2] G.H. Haertling, Ferroelectric Ceramics : History and Technology, 818 (1999) 797–818.
- [3] Y.A. Genenko, J. Glaum, M.J. Hoffmann, K. Albe, Mechanisms of aging and fatigue in ferroelectrics, Mater. Sci. Eng. B Solid-State Mater. Adv. Technol. 192 (2015) 52–82.
doi:10.1016/j.mseb.2014.10.003.
- [4] N. Balke, D.C. Lupascu, J. Granzow, Torsten, Rodel, Fatigue of Lead Zirconate Titanate Ceramics. I: Unipolar and DC Loading, 90 (2007) 1081–1087. doi:10.1111/j.1551-2916.2007.01520.x.
- [5] J. Rödel, K.G. Webber, R. Dittmer, W. Jo, M. Kimura, D. Damjanovic, Transferring lead-free piezoelectric ceramics into application, J. Eur. Ceram. Soc. 35 (2015) 1659–1681.
doi:10.1016/j.jeurceramsoc.2014.12.013.
- [6] L. Zirconate, T. Materials, Thermal Depoling Effects on Anisotropy of Lead Zirconate Titanate Materials, Society. 20 (1998) 2717–2720.
- [7] K. Takenaka, T. Maruyama, K. Sakata, (Bi_{1/2}Na_{1/2}) TiO₃-BaTiO₃ System for Lead-Free Piezoelectric Ceramics, Jpn. J. Appl. Phys. 30 (1991) 2236–2239.
- [8] G. Picht, J. Töpfer, E. Hennig, Structural properties of (Bi_{0.5}Na_{0.5})_{1-x}Ba_xTiO₃ lead-free piezoelectric ceramics, J. Eur. Ceram. Soc. 30 (2010) 3445–3453.
doi:10.1016/j.jeurceramsoc.2010.07.042.
- [9] B. Wylie-van Eerd, D. Damjanovic, N. Klein, N. Setter, J. Trodahl, Structural complexity of (Na_{0.5}Bi_{0.5})TiO₃-BaTiO₃ as revealed by Raman spectroscopy, Phys. Rev. B. 82 (2010) 104112.
doi:10.1103/PhysRevB.82.104112.
- [10] C. Xu, D. Lin, K.W. Kwok, Structure, electrical properties and depolarization temperature of (Bi_{0.5}Na_{0.5})TiO₃-BaTiO₃ lead-free piezoelectric ceramics, Solid State Sci. 10 (2008) 934–940.
doi:10.1016/j.solidstatesciences.2007.11.003.
- [11] G. Guo, R. Cross, L E, Park, S-e, Noheda, B, Cox, D E, Shirane, Origin of the High Piezoelectric Response in PbZr_{1-x}Ti_xO₃, Phys. Rev. Lett. 84 (2000) 5423–5426.
- [12] P.A. Zhang, N, Yokota, H, Glazer, A M, Ren, Z, Keen, D A, Keeble, D S, Thomas, The missing boundary in the phase diagram of PbZr_{1-x}Ti_xO₃, 5 (2014) 1–9. doi:10.1038/ncomms6231.
- [13] R.R. McQuade, M.R. Dolgos, A review of the structure-property relationships in lead-free piezoelectric (1-x)Na_{0.5}Bi_{0.5}TiO₃-(x)BaTiO₃, J. Solid State Chem. 242 (2016) 140–147.
doi:10.1016/j.jssc.2016.01.008.
- [14] A. a. Belik, Polar and nonpolar phases of BiMO₃: A review, J. Solid State Chem. 195 (2012) 32–40. doi:10.1016/j.jssc.2012.01.025.
- [15] Y. Yusa, Hitoshi, Belik, Alexei A., Takayama-Muromachi, Eiji, Hirao, Naohisa, Ohishi, High-pressure phase transitions in BiMO₃ (M=Al, Ga, and In): In situ x-ray diffraction and Raman scattering experiments, Phys. Rev. B. 80 (2009) 214103. doi:10.1103/PhysRevB.80.214103.
- [16] Z. Bai, Wangfeng, Chen, Daqin, Huang, Yanwei, Shen, Bo, Zhai, Jiwei, Ji, Electromechanical properties and structure evolution in BiAlO₃-modified Bi_{0.5}Na_{0.5}TiO₃-BaTiO₃ lead-free piezoceramics, J. Alloys Compd. 667 (2016) 6–17. doi:10.1016/j.jallcom.2016.01.144.
- [17] S.-E. Eitel, R E., Randall, C A., Shrout, T R., Rehrig, P W, Hackenberger, W, Park, New High

- Temperature Morphotropic Phase Boundary Piezoelectrics Based on Bi(Me)O₃-PbTiO₃ Ceramics, *Jpn. J. Appl. Phys.* 40 (2001) 5999–6002. doi:10.1143/JJAP.40.5999.
- [18] J. Cheng, W. Zhu, N. Li, L.E. Cross, Fabrication and characterization of xBiGaO₃–(1-x) PbTiO₃: a high temperature reduced Pb-content piezoelectric ceramic, *Mater. Lett.* 57 (2003) 2090–2094. doi:10.1016/S0167-577X(02)01143-6.
- [19] A.A. Belik, D.A. Rusakov, T. Furubayashi, E. Takayama-Muromachi, BiGaO₃-based perovskites: A large family of polar materials, *Chem. Mater.* 24 (2012) 3056–3064. doi:10.1021/cm301603v.
- [20] U. V. Baettig, P., Schelle, C. F., LeSar, R., Waghmare, N.A. Spaldin, Theoretical prediction of new high-performance lead-free piezoelectrics, *Chem. Mater.* 17 (2005) 1376–1380. doi:10.1021/cm0480418.
- [21] J. Zylberberg, A.A. Belik, E. Takayama-Muromachi, Z. Ye, Bismuth Aluminate: A New High- T C Lead-Free Piezo-/ferroelectric, *Chem. Mater.* 19 (2007) 6385–6390.
- [22] A. Ullah, C.W. Ahn, A. Hussain, I.W. Kim, Effect of BiAlO₃ concentration on the dielectric and piezoelectric properties of lead-free (Bi_{0.5}Na_{0.5})_{0.94}Ba_{0.06}TiO₃ piezoelectric ceramics, *J. Electroceramics*. 30 (2013) 82–86. doi:10.1007/s10832-012-9728-1.
- [23] M.A. Wang, Jun, Toby, Brian H., Lee, Peter L., Ribaud, Lynn, Antao, Sytle M., Kurtz, Charles, Ramanathan, Mohan, Von Dreele, Robert B., Beno, A dedicated powder diffraction beamline at the Advanced Photon Source: Commissioning and early operational results, *Rev. Sci. Instrum.* 79 (2008) 1–7. doi:10.1063/1.2969260.
- [24] A.A. Coelho, Whole-profile structure solution from powder diffraction data using simulated annealing research papers, *J. Appl. Crystallogr.* 33 (2000) 899–908. doi:10.1107/S002188980000248X.
- [25] V. V. Shvartsman, D.C. Lupascu, Lead-free Relaxor Ferroelectrics, *J. Am. Ceram. Soc.* 95 (2012) 1–26. doi:10.1111/j.1551-2916.2011.04952.x.
- [26] E.M. Anton, W. Jo, D. Damjanovic, J. Rödel, Determination of depolarization temperature of (Bi_{1/2}Na_{1/2})TiO₃-based lead-free piezoceramics, *J. Appl. Phys.* 110 (2011). doi:10.1063/1.3660253.
- [27] W. Jo, S. Schaab, E. Sapper, L.A. Schmitt, H.J. Kleebe, A.J. Bell, J. Rödel, On the phase identity and its thermal evolution of lead free (Bi_{1/2}Na_{1/2})TiO₃-6 mol BaTiO₃, *J. Appl. Phys.* 110 (2011). doi:10.1063/1.3645054.
- [28] K. Wang, A. Hussain, W. Jo, J. Rödel, Temperature-dependent properties of (Bi_{1/2}Na_{1/2})TiO₃-3- (Bi_{1/2}K_{1/2})TiO₃- SrTiO₃ lead-free piezoceramics, *J. Am. Ceram. Soc.* 95 (2012) 2241–2247. doi:10.1111/j.1551-2916.2012.05162.x.
- [29] H. Wang, H. Xu, H. Luo, Z. Yin, A.A. Bokov, Z.G. Ye, Dielectric anomalies of the relaxor-based 0.9Pb(Mg_{1/3}Nb_{2/3})O₃-0.1PbTiO₃ single crystals, *Appl. Phys. Lett.* 87 (2005) 108–111. doi:10.1063/1.1990253.
- [30] V. Bobnar, Z. Kutnjak, R. Pirc, A. Levstik, Electric-field – temperature phase diagram of the relaxor ferroelectric lanthanum-modified lead zirconate titanate, *Phys. Rev. B.* 60 (1999) 6420–6427. doi:10.1103/PhysRevB.60.6420.
- [31] A.A. Bokov, Z.G. Ye, Recent progress in relaxor ferroelectrics with perovskite structure, *J. Mater. Sci.* 41 (2006) 31–52. doi:10.1007/s10853-005-5915-7.
- [32] S. Maurya, Deepam, Pramanick, Abhijit, Feyngenson, Mikhail, Neuefeind, Joerg C., Bodnar, Robert J., Priya, Effect of poling on nanodomains and nanoscale structure in A-site disordered lead-free piezoelectric Na_{0.5}Bi_{0.5}TiO₃-BaTiO₃, *J. Mater. Chem. C.* 2 (2014) 8423–8430. doi:10.1039/C4TC01124D.
- [33] R. Garg, B.N. Rao, A. Senyshyn, P.S.R. Krishna, R. Ranjan, Lead-free piezoelectric system (Na_{0.5}Bi_{0.5})TiO₃-BaTiO₃: Equilibrium structures and irreversible structural transformations driven by electric field and mechanical impact, *Phys. Rev. B - Condens. Matter Mater. Phys.* 88 (2013) 1–15. doi:10.1103/PhysRevB.88.014103.
- [34] C. Ma, X. Tan, E. Dul'Kin, M. Roth, Domain structure-dielectric property relationship in lead-free (1-x) (Bi_{1/2}Na_{1/2})TiO₃- x BaTiO₃ ceramics, *J. Appl. Phys.* 108 (2010) 104105.

- doi:10.1063/1.3514093.
- [35] J.S. Han, Hyoungh Su, Jo, Wook, Kang, Jin Kyu, Ahn, Chang Won, Won Kim, Ill, Ahn, Kyoung Kwan, Lee, Incipient piezoelectrics and electrostriction behavior in Sn-doped Bi $1/2(\text{Na}_{0.82}\text{K}_{0.18})1/2\text{TiO}_3$ lead-free ceramics, *J. Appl. Phys.* 113 (2013) 154102. doi:10.1063/1.4801893.
 - [36] W. Jo, J. Daniels, D. Damjanovic, W. Kleemann, J. Rödel, Two-stage processes of electrically induced-ferroelectric to relaxor transition in $0.94(\text{Bi}_{1/2}\text{Na}_{1/2})\text{TiO}_3$ - 0.06BaTiO_3 , *Appl. Phys. Lett.* 102 (2013) 192903. doi:10.1063/1.4805360.
 - [37] W. Hong, Chang-Hyo, Kim, Hwang-Pill, Choi, Byung-Yul, Han, Hyoungh-Su, Son, Jae Sung, Ahn, Chang Won, Jo, Lead-free piezoceramics – Where to move on?, *J. Mater.* 2 (2016) 1–24. doi:http://dx.doi.org/10.1016/j.jmat.2015.12.002.
 - [38] J. Jo, Wook, Dittmer, Robert, Acosta, Matias, Zang, J. Groh, Claudia, Sapper, Eva, Wang, Ke, Rödel, Giant electric-field-induced strains in lead-free ceramics for actuator applications - Status and perspective, *J. Electroceramics.* 29 (2012) 71–93. doi:10.1007/s10832-012-9742-3.
 - [39] Y. Guo, Y. Liu, R.L. Withers, F. Brink, H. Chen, Large electric field-induced strain and antiferroelectric behavior in $(1-x)(\text{Na}_{0.5}\text{Bi}_{0.5})\text{TiO}_3$ - $x\text{BaTiO}_3$ ceramics, *Chem. Mater.* 23 (2011) 219–228. doi:10.1021/cm102719k.
 - [40] S.T. Zhang, A.B. Koungha, E. Aulbach, H. Ehrenberg, J. Rödel, Giant strain in lead-free piezoceramics $\text{Bi}_{0.5}\text{Na}_{0.5}\text{TiO}_3$ - BaTiO_3 - $\text{K}_{0.5}\text{Na}_{0.5}\text{NbO}_3$ system, *Appl. Phys. Lett.* 91 (2007) 2–5. doi:10.1063/1.2783200.
 - [41] S.T. Zhang, A.B. Koungha, E. Aulbach, T. Granzow, W. Jo, H.J. Kleebe, J. Rödel, Lead-free piezoceramics with giant strain in the system $\text{Bi}_{0.5}\text{Na}_{0.5}\text{TiO}_3$ - BaTiO_3 - $\text{K}_{0.5}\text{Na}_{0.5}\text{NbO}_3$. I. Structure and room temperature properties, *J. Appl. Phys.* 103 (2008) 1–9. doi:10.1063/1.2838472.
 - [42] W. Bai, D. Chen, P. Zheng, J. Zhang, F. Wen, B. Shen, J. Zhai, Z. Ji, Phase transition, switching characteristics of MPB compositions and large strain in lead-free $(\text{Bi}_{0.5}\text{Na}_{0.5})\text{TiO}_3$ -based piezoceramics, *J. Alloys Compd.* 709 (2017) 646–657. doi:10.1016/j.jallcom.2017.03.185.
 - [43] P.Y. Chen, C.S. Chen, C.S. Tu, Y.S. Wu, W.S. Chang, S.H. Chen, The giant strain response mechanism in textured Mn-modified $0.925(\text{Bi}_{0.5}\text{Na}_{0.5})\text{TiO}_3$ - 0.075BaTiO_3 relaxor ferroelectric ceramics, *J. Alloys Compd.* 737 (2018) 705–717. doi:10.1016/j.jallcom.2017.12.173.
 - [44] X. Liu, X. Tan, Giant Strains in Non-Textured $(\text{Bi}_{1/2}\text{Na}_{1/2})\text{TiO}_3$ -Based Lead-Free Ceramics, *Adv. Mater.* 28 (2016) 574–578. doi:10.1002/adma.201503768.
 - [45] A. Zaman, A. Hussain, R. Ahmed, G. Viola, H. Ning, M.J. Reece, Coexistence of ergodicity and nonergodicity in LaFeO_3 -modified, (n.d.) 0–6. doi:10.1088/0953-8984/24/36/365901.
 - [46] C. Ma, H. Guo, X. Tan, A New Phase Boundary in $(\text{Bi}_{1/2}\text{Na}_{1/2})\text{TiO}_3$ – BaTiO_3 Revealed via a Novel Method of Electron Diffraction Analysis, *Adv. Funct. Mater.* 23 (2013) 5261–5266. doi:10.1002/adfm.201300640.
 - [47] B. Noheda, Structure and high-piezoelectricity in lead oxide solid solutions, *Curr. Opin. Solid State Mater. Sci.* 6 (2002) 27–34.
 - [48] D. Ge, Wenwei, Luo, Chengtao, Zhang, Qinhui, Ren, Yang, Li, Jiefang, Luo, Haosu, Viehland, Evolution of structure in $\text{Na}_{0.5}\text{Bi}_{0.5}\text{TiO}_3$ single crystals with BaTiO_3 , *Appl. Phys. Lett.* 105 (2014) 162913. doi:10.1063/1.4900547.
 - [49] M.R. Aksel, Elena, Forrester, Jennifer S., Jones, Jacob L., Thomas, Pam A., Page, Katharine, Suchomel, Monoclinic crystal structure of polycrystalline $\text{Na}_{0.5}\text{Bi}_{0.5}\text{TiO}_3$, *Appl. Phys. Lett.* 98 (2011) 152901. doi:10.1063/1.3573826.
 - [50] A.M. Glazer, The classification of tilted octahedra in perovskites, *Acta Cryst.* B28 (1972) 3384. doi:10.1107/S0567740872007976.
 - [51] R. Ranjan, A. Dwiwedi, Structure and dielectric properties of $(\text{Na}_{0.50}\text{Bi}_{0.50})_{1-x}\text{Ba}_x\text{TiO}_3$, *Solid State Commun.* 135 (2005) 394–399. doi:10.1016/j.ssc.2005.03.053.
 - [52] T.-M. Usher, J.S. Forrester, C.R. dela Cruz, J.L. Jones, Crystal structure of $0.96(\text{Na}_{0.5}\text{Bi}_{0.5}\text{TiO}_3)$ – $0.04(\text{BaTiO}_3)$ from combined refinement of x-ray and neutron diffraction patterns, *Appl. Phys. Lett.* 101 (2012) 152906. doi:10.1063/1.4759117.

- [53] I. Levin, I.M. Reaney, Nano- and Mesoscale Structure of $\text{Na}_{1/2}\text{Bi}_{1/2}\text{TiO}_3$: A TEM Perspective, *Adv. Funct. Mater.* (2012) 3445–3452.
- [54] D. Yao, Jianjun, Monsegue, Niven, Murayama, Mitsuhiro, Leng, Weinan, Reynolds, William T., Zhang, Qinhui, Luo, Haosu, Li, Jiefang, Ge, Wenwei, Viehland, Role of coexisting tetragonal regions in the rhombohedral phase of $\text{Na}_{0.5}\text{Bi}_{0.5}\text{TiO}_3$ -x at.% BaTiO_3 crystals on enhanced piezoelectric properties on approaching the morphotropic phase boundary, *Appl. Phys. Lett.* 100 (2012) 012901. doi:10.1063/1.3673832.
- [55] C. Ma, H. Guo, S.P. Beckman, X. Tan, Creation and destruction of morphotropic phase boundaries through electrical poling: A case study of lead-free $(\text{Bi}_{1/2}\text{Na}_{1/2})\text{TiO}_3$ - BaTiO_3 piezoelectrics, *Phys. Rev. Lett.* 109 (2012) 107602. doi:10.1103/PhysRevLett.109.107602.
- [56] S. Maurya, Deepam, Murayama, M., Pramanick, A., Reynolds, W. T., An, Ke, Priya, Origin of high piezoelectric response in A-site disordered morphotropic phase boundary composition of lead-free piezoelectric $0.93(\text{Na}_{0.5}\text{Bi}_{0.5})\text{TiO}_3$ - 0.07BaTiO_3 , *J. Appl. Phys.* 113 (2013) 114101. doi:10.1063/1.4792729.
- [57] M.E.A. De Dompablo, G. Ceder, First-principles calculations on Li_xNiO_2 : phase stability and monoclinic distortion, *J. Power Sources.* 121 (2003) 654–657. doi:10.1016/S0378-7753(03)00199-X.
- [58] A.A. Bokov, Z. Ye, Universal relaxor polarization in $\text{Pb}(\text{Mg}_{1/3}\text{Nb}_{2/3})\text{O}_3$ and related materials, *Phys. Rev. B.* 66 (2002) 064103. doi:10.1103/PhysRevB.66.064103.
- [59] D. Maurya, A. Pramanick, K. An, S. Priya, Enhanced piezoelectricity and nature of electric-field induced structural phase transformation in textured lead-free piezoelectric $\text{Na}_{0.5}\text{Bi}_{0.5}\text{TiO}_3$ - BaTiO_3 ceramics, *Appl. Phys. Lett.* 100 (2012) 172906. doi:10.1063/1.4709404.
- [60] R. Garg, B.N. Rao, A. Senyshyn, R. Ranjan, Long ranged structural modulation in the pre-morphotropic phase boundary cubic-like state of the lead-free piezoelectric $\text{Na}_{1/2}\text{Bi}_{1/2}\text{TiO}_3$ - BaTiO_3 , *J. Appl. Phys.* 114 (2013) 234102. doi:10.1063/1.4842855.
- [61] J.E. Daniels, W. Jo, J. Roedel, J.L. Jones, Electric-field-induced phase transformation at a lead-free morphotropic phase boundary. Case study in a 93% $(\text{Bi}_{0.5}\text{Na}_{0.5})\text{TiO}_3$ -7% BaTiO_3 piezoelectric ceramic, *Appl. Phys. Lett.* 95 (2009) 032904. doi:10.1063/1.3182679.
- [62] J.Z. Wangfeng Bai, Peng Li, Lingyu Li, Jingji Zhang, Bo Shen, Structure evolution and large strain response in BNT e BT lead-free, *J. Alloys Compd.* 649 (2015) 772–781. doi:10.1016/j.jallcom.2015.07.178.
- [63] W.Z. Jin, C C, Wang, F F, Yao, Q R, Tang, Y X, Wang, T, Shi, Ferroelectric , dielectric properties and large strain response in Zr-modified, *Ceram. Int.* 40 (2014) 6143–6150. doi:10.1016/j.ceramint.2013.11.066.
- [64] T.K.S. Jamil Ur Rahmana, Ali Hussain a, Adnan Maqboola, Gyung Hyun Ryua, M.H.K. Won-Jeong Kimb, Field induced strain response of lead-free BaZrO_3 -modified $\text{Bi}_{1/2}\text{Na}_{1/2}\text{TiO}_3$ - BaTiO_3 ceramics, *J. Alloys Compd.* 593 (2014) 97–102. doi:10.1016/j.jallcom.2014.01.031.
- [65] M. Maqbool, Adnan, Hussain, Ali, Ur, Jamil, Kwon, Tae, Kim, Won-jeong, Lee, Jehyun, Kim, Enhanced electric field-induced strain and ferroelectric behavior of $(\text{Bi}_{0.5}\text{Na}_{0.5})\text{TiO}_3$ - BaTiO_3 - SrZrO_3 lead-free ceramics, *Ceram. Int.* 40 (2014) 11905–11914. doi:10.1016/j.ceramint.2014.04.026.
- [66] and C.M.L. Feifei Wang, Min Xu, Yanxue Tang, Tao Wang, Wangzhou Shi, Large Strain Response in the Ternary $\text{Bi}_{0.5}\text{Na}_{0.5}\text{TiO}_3$ - BaTiO_3 - SrTiO_3 Solid Solutions, *J. Am. Ceram. Soc.* 95 (2012) 1955–1959. doi:10.1111/j.1551-2916.2012.05119.x.
- [67] C.C. Jin, F.F. Wang, L.L. Wei, J. Tang, Y. Li, Q.R. Yao, C.Y. Tian, W.Z. Shi, Influence of B-site complex-ion substitution on the structure and electrical properties in $\text{Bi}_{0.5}\text{Na}_{0.5}\text{TiO}_3$ -based lead-free solid solutions, *J. Alloys Compd.* 585 (2014) 185–191. doi:10.1016/j.jallcom.2013.09.152.
- [68] R.F. Ge, Z.H. Zhao, S.F. Duan, X.Y. Kang, Y.K. Lv, D.S. Yin, Y. Dai, Large electro-strain response of La^{3+} -and Nb^{5+} -co-doped ternary $0.85\text{Bi}_{0.5}\text{Na}_{0.5}\text{TiO}_3$ - $0.11\text{Bi}_{0.5}\text{K}_{0.5}\text{TiO}_3$ - 0.04BaTiO_3 lead-free piezoelectric ceramics, *J. Alloys Compd.* 724 (2017) 1000–1006. doi:10.1016/j.jallcom.2017.07.086.

- [69] T.-M. Usher, J.S. Forrester, C.R. dela Cruz, J.L. Jones, Crystal structure of $0.96(\text{Na}_{0.5}\text{Bi}_{0.5}\text{TiO}_3)-0.04(\text{BaTiO}_3)$ from combined refinement of x-ray and neutron diffraction patterns, *Appl. Phys. Lett.* 101 (2012) 152906. doi:10.1063/1.4759117.

Highlights

- Synthesized new NBT-BT type compositions
- Some compositions have higher strain properties than the parent compound
- incipient piezoelectricity could lead to high performing materials.